ACS APPLIED MATERIALS & INTERFACES

Research Article

www.acsami.org

Self-Assembled Nanoparticles Based on PEGylated Conjugated Polyelectrolyte and Drug Molecules for Image-Guided Drug Delivery and Photodynamic Therapy

Youyong Yuan[†] and Bin Liu*[,†,‡]

[†]Department of Chemical and Biomolecular Engineering, National University of Singapore, 4 Engineering Drive 4, Singapore 117585, Singapore

[‡]Institute of Materials Research and Engineering, 3 Research Link, Singapore 117602, Singapore

ABSTRACT: A drug delivery system based on poly(ethylene glycol) (PEG) grafted conjugated polyelectrolyte (CPE) has been developed to serve as a polymeric photosensitizer and drug carrier for combined photodynamic and chemotherapy. The amphiphilic brush copolymer can self-assemble into micellar nanopaticles (NPs) in aqueous media with hydrophobic conjugated polyelectrolyte backbone as the core and hydrophilic PEG as the shell. The NPs have an average diameter of about 100 nm, with the absorption and emission maxima at 502 and 598 nm, respectively, making them suitable for bioimaging applications. Moreover, the CPE itself can serve as a photosensitizer, which makes the NPs not only a carrier for drug but also a photosensitizing unit for photodynamic therapy, resulting in the combination of chemo- and photodynamic therapy for cancer. The half-maximal inhibitory concentration (IC_{50}) value for the combination therapy to U87-MG cells is 12.7 μg mL^{-1}, which is much lower than that for the solely photodynamic therapy (25.5 μg mL^{-1}) or chemotherapy (132.8 μg mL^{-1}). To improve the tumor specificity of the system, cyclic arginine-glycine-aspartic acid (cRGD) tripeptide as the receptor to integrin $\alpha_v\beta_3$ overexpressed cancer cells was further incorporated to the surface of the NPs. The delivery system based on PEGylated CPE is easy to fabricate, which integrates the merits of targeted cancer cell image, chemotherapeutic drug delivery, and photodynamic therapy, making it promising for cancer treatment.

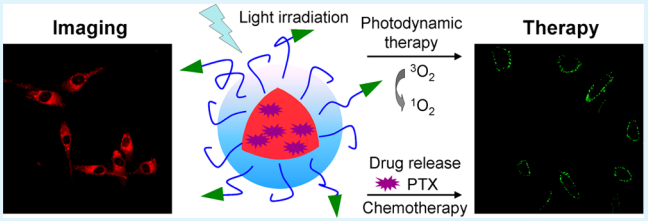

KEYWORDS: *conjugated polyelectrolyte, photodynamic therapy, drug delivery, theranostic, cancer therapy*

INTRODUCTION

Polymeric nanoparticles (NPs) have recently received broad attention as a promising vehicles for drug delivery.[1] These systems exhibit many advantages for biomedical applications such as favorable biodistribution, long circulation, high therapeutic effects, and low side effects of the drugs, which have been widely used for chemotherapy, gene therapy, photothermal therapy, photodynamic therapy (PDT), and so on.[2−6] However, cancer therapy with single therapeutic modality often fails to kill cancer cells completely.[7] The combination of different therapeutic modalities can significantly enhance the therapeutic efficiency as compared to solely treatment, which is a promising alternative for cancer therapy.[8−11] Among them, PDT has gained increasingly attention in cancer therapy, which is based on the generation of toxic reactive oxygen species (ROS) upon light irradiation of a photosensitizer.[12,13] The combination of PDT and chemotherapy has been reported to induce antitumor immunity and revert multidrug resistance of cancer cells.[14] To achieve the combination therapy, photosensitizers and chemotherapeutic drugs are typically coloaded into one delivery system.[15−18] However, photosensitizers, such as porphyrin derivatives, could aggregate easily due to $\pi-\pi$ interactions, resulting in a dramatic reduction in ROS generation with reduced PDT efficiency. To solve this problem, Son et al. developed a drug delivery system based on dendritic porphyrin, which serves not only as the photosensitizer with reduced self-quenching but also as a matrix for drug delivery to achieve the combination of photodynamic therapy and chemotherapy.[17] As each dendrimer only contains one photosensitizer molecule, the low sensitizer concentration could comprise the therapeutic effect.

Light-harvesting conjugated polyelectrolytes (CPEs) with π-delocalized backbones have been widely used in biological sensing and imaging applications.[19−24] Recently, it has also been reported that CPEs with specific structures can generate ROS efficiently under light irradiation.[25−27] These inherent properties inspired us to develop a drug delivery system based on a PEGylated CPE, which can be used not only as a matrix for drug delivery but also as a photosensitizing unit for photodynamic therapy. In addition to therapeutic function, the inherent fluorescence of CPE also provides the opportunity for image-guided chemo- and photodynamic therapy. In this contribution, we developed a multifunctional NP based on PEGylated CPE, which serves as a chemotherapeutic drug

Received: April 6, 2014
Accepted: July 30, 2014
Published: July 30, 2014

   dx.doi.org/10.1021/am5020925 | *ACS Appl. Mater. Interfaces* 2014, 6, 14903−14910

carrier for targeted cancer cell imaging and chemo-, photodynamic therapy. The PEGylated CPE can easily self-assemble into NPs in aqueous media, which can encapsulate commonly used hydrophobic chemotherapeutic drugs, such as paclitaxel (PTX), through hydrophobic−hydrophobic interaction. In addition, the polymer matrix itself can also serve as a photosensitizer for imaging and photodynamic therapy. To improve the specificity of the system, recognition element cyclic arginine-glycine-aspartic acid (cRGD) tripeptide, which can target integrin $\alpha_v\beta_3$ overexpressed cancer cells, was incorporated onto the self-assembled NPs for targeted cancer therapy.[28] By combining these capabilities, the drug-loaded PEGylated CPE platform has the following distinct advantages: (1) easy to fabricate; (2) image-guided therapy; (3) dual therapy (photodynamic therapy and chemotherapy); and (4) target ability (Scheme 1).

Scheme 1. Chemical Structure (A) and NP Fabrication Using PFVBT-*g*-PEG As Carrier for a Hydrophobic Anticancer Drug (Paclitaxel, PTX) To Realize Image-Guided Combination of Chemotherapy and Photodynamic Therapy

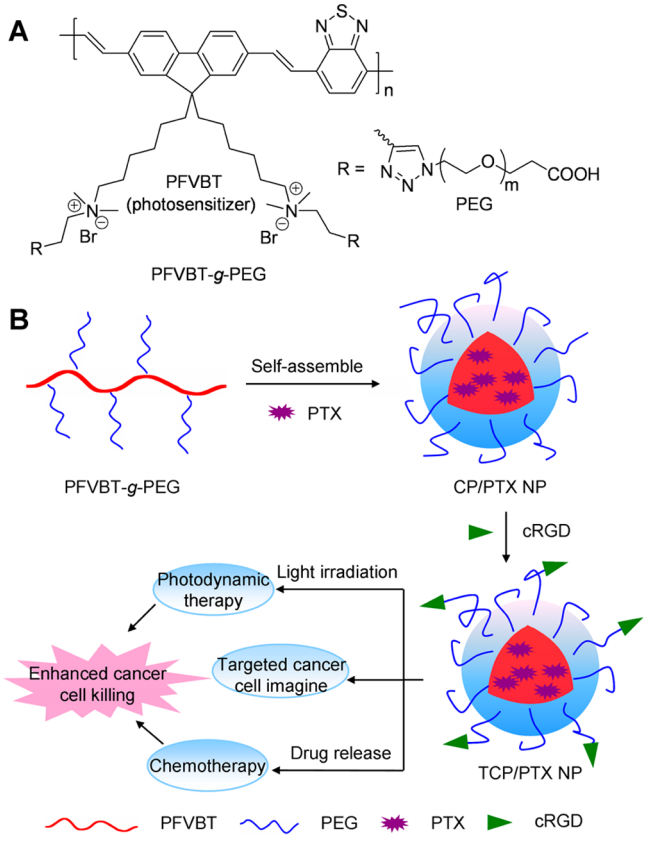

EXPERIMENTAL SECTION

Reagents and Chemicals. α-Azide-ω-caboxyl-poly(ethylene glycol) (N_3-PEG-COOH, average molecule weight of 3400) was purchased from Nanocs Inc. (U.S.A.). Paclitaxel (PTX) was purchase from Santa Cruz Biotechnology, Inc. All the other chemicals used in this work were purchased from Sigma-Aldrich. Dulbecco's Modified Essential Medium (DMEM) was purchased from Invitrogen. Annexin V-FITC apoptosis detection kit, Fetal bovine serum (FBS) and trypsin-EDTA solution were purchased from Life Technologies. Peptide with a sequence of cyclic(Arg-Gly-Asp-D-Phe-Lys)) was purchased from GL Biochem (Shanghai, China). Poly[9,9-bis(*N*-(but-3′-ynyl)-*N*,*N*-dimethylamino)hexyl))fluorenyldivinylene-*alt*-4,7-(2′,1′,3′,-benzothiadiazole) dibromide] (PFVBT, M_n = 8,700, M_w/M_n = 2.3) was synthesized according to the literature.[29,30]

The dialysis membrane and the Milli-Q Plus System were supplied by Millipore Corporation (Bedford, U.S.A.). Milli-Q water (18.2 MΩ) was used for all the experiments. 1× PBS containing KCl (2.7 mM), NaCl (137 mM), Na_2HPO_4 (10 mM), and KH_2PO_4 (1.8 mM) was prepared from 10× PBS stock buffer (first BASE, Singapore).

Instrumentation. The sizes and morphology of nanoparticles were studied by laser light scattering (LLS, Brookhaven Instruments Co., U.S.A.) and transmission electron microscope (TEM, JEOL JEM-2010). HPLC analyses were performed using an Agilent HPLC system. UV−vis absorption spectra were taken on a Shimadzu Model UV-1700 spectrometer. Fluorescence measurements were recorded on a PerkinElmer LS 55 spectrofluorometer. All UV and PL spectra were collected at 24 ± 1 °C.

Preparation of NPs Loaded with PTX (CP/PTX NPs). PFVBT-*g*-PEG NPs and PTX-loaded NPs were prepared by a dialysis method. Briefly, PFVBT-*g*-PEG (5 mg) with PTX (0−300 μg mL^{-1}) were first dissolved in DMSO (2 mL) and stirred at room temperature for 2 h. Milli-Q water (10 mL) was added dropwise to the above solution with stirring. After stirring at room temperature for additional 1 h, the solvent was removed through dialysis (MWCO 3500 Da). The solution was filtered using a 0.45 μm filter and stored at 4 °C for further experiments.

Conjugation of Target Moiety cRGD to the CP/PTX NPs Surface. cRGD modified CP/PTX NPs were prepared by adding 1-ethyl-3-[3-(dimethylamino)propyl]carbodiimide hydrochloride (EDC, 10 mM) and *N*-hydroxysulfosuccinimide sodium salt (sulfo-NHS, 5 mM) to the CP/PTX NPs (0.2 mg mL^{-1}) and incubated for 30 min. The obtained sulfo-NHS activated CP/PTX NPs were washed with water by ultrafiltration (MWCO 20 000). Then, the activated NPs were reacted with amine functionalized cRGD (1 mg mL^{-1}) for 4 h under magnetic stirring. The cRGD functionalized NPs were washed with water by ultrafiltration for 10 min (1000 g), and resuspended in water for further use. The obtained targeted NPs were denoted as TCP/PTX NPs.

Detection of ROS in Solution. A ROS-sensitive probe, dichlorfluorescein diacetate (DCF-DA), was used in our experiment to detect the ROS generation from NPs under light irradiation according to a similar procedure reported before.[31] The CP/PTX NPs in DCF-DA solution (0.1 mg mL^{-1}) was exposed to light irradiation (0.1 W cm^{-2}) for designated time. The fluorescence change in the solution was measured with excitation at 488 nm.

Determination of Drug Content. CP/PTX NPs were dissolved in DMSO/water (v/v = 50/50) and measured by HPLC to determine PTX content. HPLC analyses were performed using acetonitrile−water (50:50, v/v) with 0.1% trifluoroacetic acid as the eluent. The PTX absorption at 227 nm was compared with the linear calibration curve (0.5−300 μg mL^{-1}). Drug loading content (DLC) and drug loading efficiency (DLE) of PTX based on CPE was calculated as follows: DLC (%) = [PTX in PFVBT-*g*-PEG]/[PFVBT-*g*-PEG] × 100. DLE (%) = [PTX in PFVBT-*g*-PEG]/[PTX used for encapsulation] × 100.

In Vitro Drug Release. Release of PTX from the NPs was evaluated in PBS (pH 7.4) using dialysis membrane tubing (MWCO 3500 Da). PTX-loaded NPs were added into the dialysis membrane tubing and placed into PBS (20 mL) and incubated at 37 °C. At designated time, the dialysis tube was placed into another fresh medium. The PTX concentration in the release medium was studied by HPLC.

Cell Culture. U87-MG and MCF-7 cells were provided by American Type Culture Collection (ATCC) and cultured in DMEM containing 10% heat-inactivated FBS (Invitrogen), 100 U mL^{-1} penicillin, and 100 μg/mL streptomycin at 37 °C with 5% CO_2. The cells were precultured until confluence was reached before each experiment.

ROS Detection in Cells. ROS generation in cells upon light irradiation was studied using DCF-DA as the indicator. U87-MG cells were precultured in the chambers overnight at 37 °C. After 80% confluence, the culture medium was removed and washed twice with

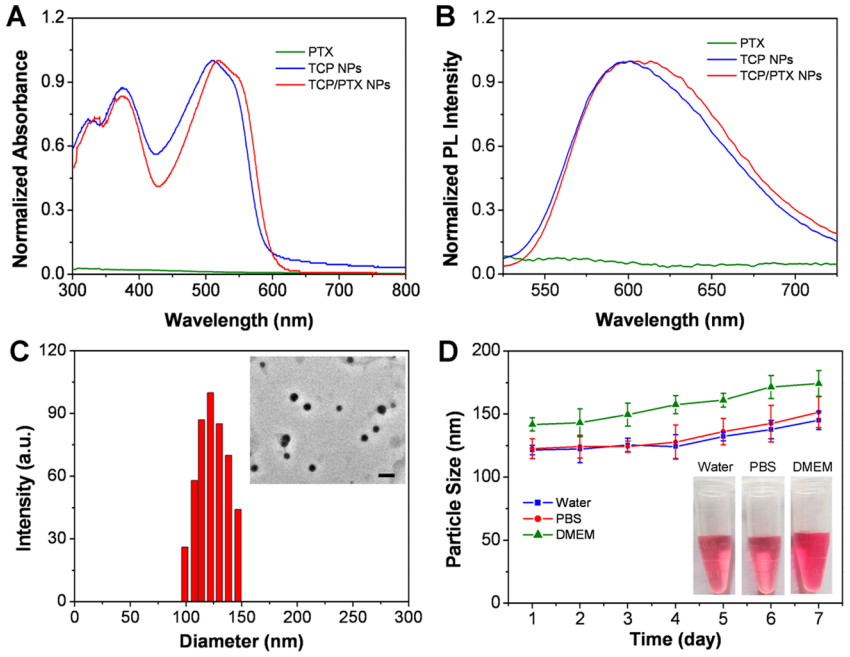

Figure 1. (A) Normalized absorption spectra of PTX, TCP NPs, and TCP/PTX NPs. (B) Normalized emission spectra of PTX, TCP NPs, and TCP/PTX NPs upon excitation at 502 nm. (C) LLS result of TCP/PTX NPs. The inset shows the TEM image. The scale bar is 200 nm. (D) Size change of TCP/PTX NPs upon incubation in different media at 37 °C for 7 days.

PBS buffer. Following incubation with TCP/PTX NPs (10 μg mL^{-1}) for 4 h in the dark and washed with PBS, DCF-DA in fresh medium was added, and the cells were incubated for additional 10 min. Then the cells were washed with PBS and exposed to white light irradiation (0.1 W cm^{-2}) for 5 min. In some experiments, vitamin C (50 μM) was added as a scavenger of ROS. After irradiation, the medium was replaced with PBS and studied by a confocal microscope. For TCP/PTX NPs detection, the excitation was 488 nm, and the emission was collected at 591 ± 10 nm; for DCF detection, the excitation was 488 nm, and the emission was collected at 511 ± 10 nm.

Confocal Imaging. MCF-7 and U87-MG cells were precultured in the chambers overnight at 37 °C. After 80% confluence, the cells were washed twice with PBS buffer. Following incubation with TCP/PTX NPs (10 μg mL^{-1}) for 4 h, the cell nuclei were living stained with Hoechst 33342 (Life Technologies) following the standard protocol of the manufacturer. The cellular apoptosis imaging measurement was carried out based on standard detection kit (Annexin V-FITC) according to manufacturer's protocol. The cells were then imaged by a confocal microscope and analyzed by ImageJ 1.43 × program. For TCP/PTX NPs detection, E_x = 488 nm; E_m = 591 ± 10 nm. For FITC detection, E_x = 488 nm; E_m = 511 ± 10 nm. For Hoechst, E_x = 405 nm; E_m = 466 ± 10 nm.

Quantification of the Cellular Uptake of the NPs. MCF-7 and U87-MG cells were seeded in 96-well plates and incubated with TCP/PTX NPs (10 μg mL^{-1}) in fresh FBS-free DMEM medium. After the designated time, the cells were washed with 1× PBS and the fluorescence was studied by a microplate reader (E_x = 488 nm; E_m = 598 nm).

Cytotoxicity Studies. Cell viability was evaluated using standard 3-(4,5-dimethythiazol-2-yl)-2,5-diphenyltetrazolium bromide (MTT) assays. Cells seeded in 96-well plates were precultured overnight and incubated with the NPs in fresh medium. After incubated for 2 h, the cells were washed with PBS and irradiated with light (10 min, 0.1 W cm^{-2}). After a further incubation for 24 h, the cells were treated with MTT solution (100 μL, 0.5 mg mL^{-1} in PBS) for 3 h. Then, 100 μL of DMSO was added to each well. The absorbance of MTT at 570 nm was studied using a microplate reader. Cell viability was calculated by comparing the absorbance of the cells treated with NPs to that of the cells without any treatment.

Lactate Dehydrogenase (LDH) Measurements. The LDH leakage studies were performed with LDH detection kit (Promega) using the manufacture's protocol. After NP incubation, the cells were treated with the kit for 30 min at room temperature and the LDH activity was determined by monitoring absorbance at 490 nm using a microplate reader (Bio-Rad). Cells treated with 1% Triton X-100 and without any treatment were used as the positive and negative controls, respectively.

RESULTS AND DISCUSSION

Alkyne functionalized PFVBT was synthesized according to literatrue.[29,30] Subsequent click reaction between the polymer and α-azide-ω-caboxyl-poly(ethylene glycol) (N_3−PEG-COOH) using copper(I) bromide (CuBr) and *N,N,N′,N″,N‴*-pentametyldiethylenetriamine as the catalyst yielded the PEGylated brush copolymer of PFVBT-*g*-PEG. The grafting efficiency was calculated to be 79% based on NMR analysis.[30]

The PFVBT-*g*-PEG with hydrophobic backbone and hydrophilic PEG side chains can self-assemble into NPs in aqueous solution. The NPs encapsulated with hydrophobic anticancer drug paclitaxel (PTX) were prepared by a dialysis method to yield CP/PTX NPs. The surface of the NPs was further functionalized with a cancer targeting cRGD tripeptide (denoted as TCP/PTX NPs) for targeted drug delivery. The targeted NPs without PTX loading (denoted as TCP NPs) were also prepared under the same conditions. Figure 1A shows the absorption spectra of PTX, TCP NPs, TCP/PTX NPs in water. The TCP/PTX NPs have an absorption maximum at 502 nm with an emission maximum of 598 nm. The size and distribution of TCP/PTX NPs were studied by LLS. The NPs show an average diameter of 128 ± 13.4 nm (Figure 1C). The morphology of the TCP/PTX NPs was further studied by TEM. As shown in Figure 1C, the TCP/PTX NPs show an average diameter of about 100 nm with a spherical shape. The stability of the TCP/PTX NPs was also studied. As shown in Figure 1D, the TCP/PTX NPs are well dispersed in different

dx.doi.org/10.1021/am5020925 | ACS Appl. Mater. Interfaces 2014, 6, 14903−14910

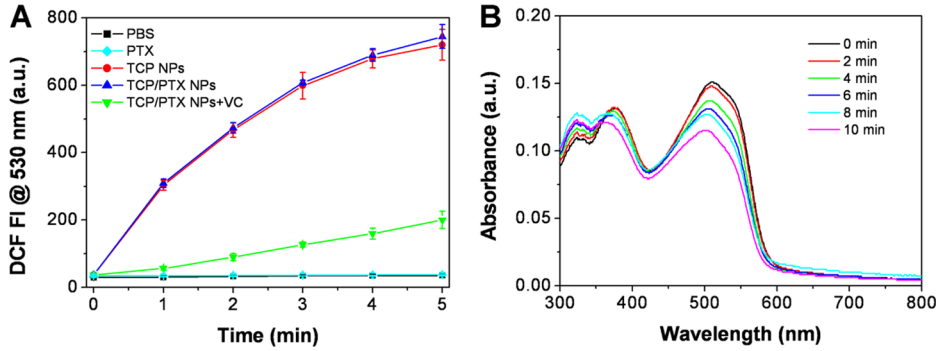

Figure 2. (A) Fluorescence intensity (Fl) change at 530 nm for dichlorofluorescin (DCF) in PBS, PTX, TCP/PTX NPs, and TCP NPs after light irradiation for different time. VC is Vitamin C. (B) Light irradiation induced absorbance change of TCP NPs after irradiation for different time (0.1 W cm^{-2}).

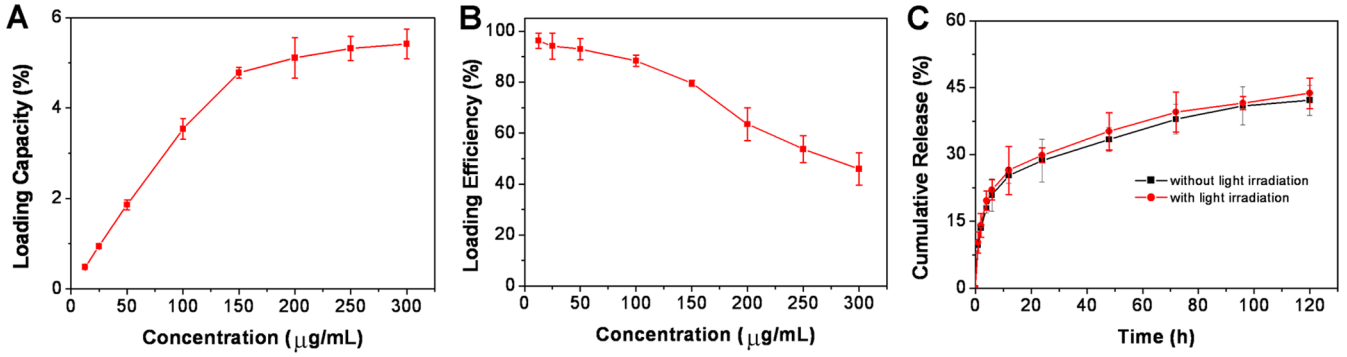

Figure 3. Loading capacity and loading efficiency of PTX in PFVBT-*g*-PEG NPs and the drug release in PBS solution. (A) PTX loading capacity at various drug concentrations; (B) Loading efficiency of PTX in TCP/PTX NPs at different drug concentrations; (C) cumulative drug release profiles for TCP/PTX NPs in the presence and absence of light irradiation (10 min, 0.1 W cm^{-2}). [PFVBT-*g*-PEG] = 2.5 mg mL^{-1}.

media. Moreover, the diameters of TCP/PTX NPs showed little change even after 1 week incubation in different media, demonstrating good colloidal stability of the TCP/PTX NPs.

We also studied the ROS generation for TCP NPs and TCP/PTX NPs. The ROS generation was evaluated by using a fluorescent ROS indicator, dichlorofluorescein diacetate (DCF-DA). It is nonfluorescent, but the oxidized product (dichlorofluorescein, DCF) can emit strong fluorescence. As shown in Figure 2A, the fluorescence intensity at 530 nm increased greatly upon white light irradiation (0.1 W cm^{-2}, 5 min) of the mixture solution of DCF-DA and TCP/PTX NPs. However, the fluorescence intensity of DCF-DA solution with PTX maintained at the original level, indicating that the ROS is generated by the polymer matrix upon light irradiation. In addition, the loading of PTX in the TCP/PTX NPs has a minimum interference with ROS production. When ROS scavenger vitamin C (VC) was added, the fluorescence signal of DCF in the solution was remarkably inhibited, further confirming the ROS generation by the TCP/PTX NPs upon light irradiation. TCP NPs show reasonably good photostability as there is less than 20% absorbance change after continuous irradiation for 10 min by a 0.1 W cm^{-2} white light source (Figure 2B). It is also important to note that there is no change in the absorption spectrum when the TCP NPs are stored in aqueous media at room temperature in the absence of light for several weeks.

To evaluate the applications of PFVBT-*g*-PEG NPs for drug delivery, hydrophobic anticancer drug PTX was encapsulated into the NPs and the drug loading and release properties were studied. The drug loading content (DLC) and efficiency (DLE) were quantitatively measured by HPLC analysis. DLC and DLE of PTX based on CPE were calculated as follows: DLC (%) = [PTX in PFVBT-*g*-PEG]/[PFVBT-*g*-PEG] × 100. DLE (%) = [PTX in PFVBT-*g*-PEG]/[PTX used for the encapsulation] × 100. As shown in Figure 3A, with the increased concentrations of PTX used, the DLC increases steadily and reach a plateau at 5.4% when the PTX concentration is 200 μg mL^{-1}. On the other hand, the DLE of PTX in the NPs gradually reduces with the increased PTX concentration (Figure 3B). The DLE is about 45.9% at the PTX concentration of 300 μg mL^{-1}, indicating that PFVBT-*g*-PEG NPs are good carriers for hydrophobic drugs. It is also found that the DLC and DLE of the TCP/PTX NPs were affected by PTX concentration used. The in vitro PTX release from the TCP/PTX NPs was performed using PBS (0.01 M, pH 7.4) at 37 °C as the release medium. As shown in Figure 3C, the in vitro release profiles of TCP/PTX NPs with and without light irradiation are similar, and nearly 40% of PTX is released within 72 h. The results suggest that the light irradiation does not evidently influence the in vitro release behavior of PTX from the NPs. In addition, the sustained release of PTX over a long time will facilitate the continuous toxicity to cancer cells.

Cancer-targeted delivery systems are promising to achieve better therapeutic efficiency for cancer therapy through active accumulation in tumor site. In this work, U87-MG and MCF-7 cells with different degrees of $\alpha_v\beta_3$ integrin expression were used as integrin-positive and negative cells, respectively. We incubated the TCP/PTX NPs with both cells and the CPE fluorescence was measured at designated time. As shown in Figure 4, red fluorescence of CPE and blue fluorescence from

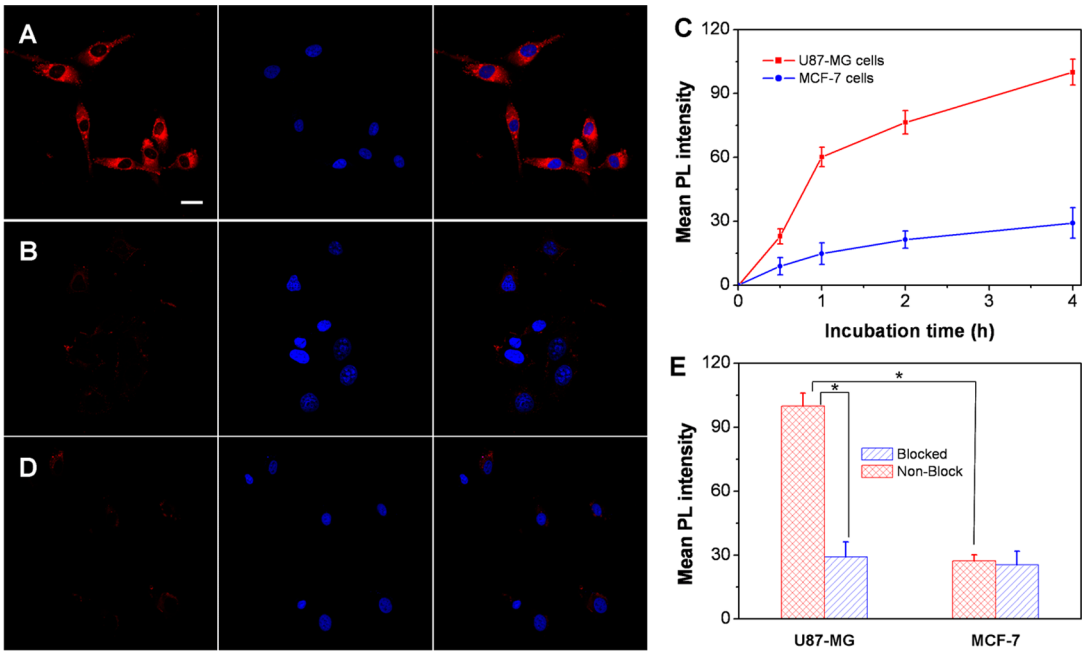

Figure 4. Selective imaging of TCP/PTX NPs incubated with U87-MG and MCF-7 cells: (A–B) confocal microscopy images of NPs uptake in U87-MG cells (A) with receptor overexpression and receptor negative MCF-7 cells (B). The blue fluorescence from the nuclei of cells is dyed by Hoechst 33342, the red fluorescence is from TCP/PTX NPs, and the overlay images of above. The scale bar is 20 μm. (C) Dynamic fluorescence intensity of TCP/PTX NPs determined in MCF-7 and U87-MG cells at different incubation time points. (D) confocal microscopy images of TCP/PTX NPs uptake in cRGD (50 μM) pretreated U87-MG cells and (E) mean fluorescence intensity of TCP/PTX NPs determined in MCF-7 and U87-MG cells with receptor blocking or nonblocking after 4 h incubation ($P < 0.05$). For TCP/PTX NPs detection, the excitation was 488 nm, and the emission was collected at 591 ± 10 nm; for Hoechst, the excitation was 405 nm, and the emission was collected at 466 ± 10 nm.

Hoechst stained nucleus were observed in U87-MG cells (Figure 4A) with elevated $\alpha_v\beta_3$ integrin expression after 4 h incubation. In addition, at each time point, the red fluorescence in U87-MG cells is much stronger than that in MCF-7 cells (Figure 4B). Semiquantitative analysis confirmed that the red fluorescence from U87-MG cells is about 3.6-fold higher than that in MCF-7 cells (Figure 4C). However, when the cells are pretreated with free cRGD before the TCP/PTX NPs incubation, the fluorescence intensity of CPE dramatically reduces in U87-MG cells (Figure 4D), indicating that the TCP/PTX NPs are uptaken through a $\alpha_v\beta_3$ integrin receptor mediated endocytosis. As shown in Figure 4E, semiquantitative fluorescence analysis in U87-MG demonstrates that there is significant difference ($p < 0.05$) in the cellular uptake of TCP/PTX NPs between the cells pretreated with and without free cRGD. For MCF-7 cells, there is no significant difference when the receptor is blocked or not.

The ROS generation of TCP/PTX NPs after entering the cells upon light irradiation was also studied by using DCF-DA. As shown in Figure 5, the fluorescence of DCF (green) is negligible when the cells are incubated with DCF-DA or the NPs with the light irradiation. In contrast, after loading of DCF-DA in TCP/PTX NPs incubated cells, strong green fluorescence ascribe to DCF can be observed, indicating the ROS generation inside the cells. However, the fluorescence is greatly inhibited when the ROS scavenger vitamin C is added, further confirming that the fluorescence increase is due to the oxidation of DCF-DA by ROS.

The biocompatibility is a prerequisite property of a drug delivery system. We first tested the in vitro toxicity of the PFVBT-*g*-PEG nanoparticles without PTX loading (TCP NPs) in the dark. The MTT assay was utilized to study the toxicity of TCP NPs to MCF-7 and U87-MG cells. As shown in Figure

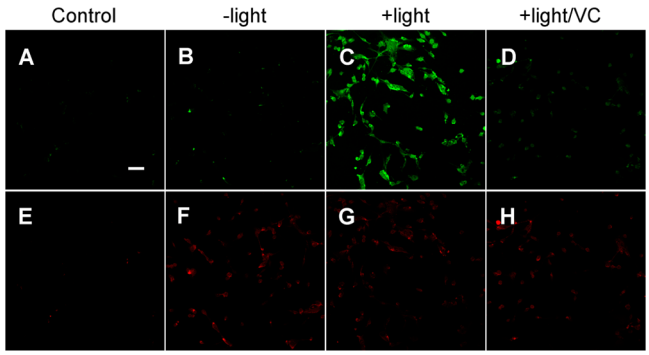

Figure 5. Intracellular ROS detection in U87-MG cells using DCF-DA as the indicator. U87-MG cells incubated with (A) DCF-DA with white light irradiation; (B) TCP/PTX NPs without white light irradiation; (C) TCP/PTX NPs and DCF-DA with light irradiation; (D) TCP/PTX NPs and DCF-DA in the presence of ROS scavenger vitamin C (VC, 50 μM) with light irradiation. (E–H) Corresponding TCP/PTX NPs fluorescence images. The scale bar is 50 μm. For TCP/PTX NPs detection, the excitation was 488 nm, and the emission was collected at 591 ± 10 nm; for FITC detection, the excitation was 488 nm, and the emission was collected at 511 ± 10 nm.

6A–B, no obvious toxicity of TCP NPs is observed for both cells up to a concentration of 0.2 mg mL^{-1}. To further evaluate any potential damage of cell membrane caused by the TCP NPs, the LDH leakage from the cells was studied. As shown in Figures 6C–D, the LDH leakage from U87-MG and MCF-7 cells after incubation with the TCP NPs is comparable to that of the cells without any treatment, indicating the integrity of the cell membrane. The cell viability assay and the cell membrane

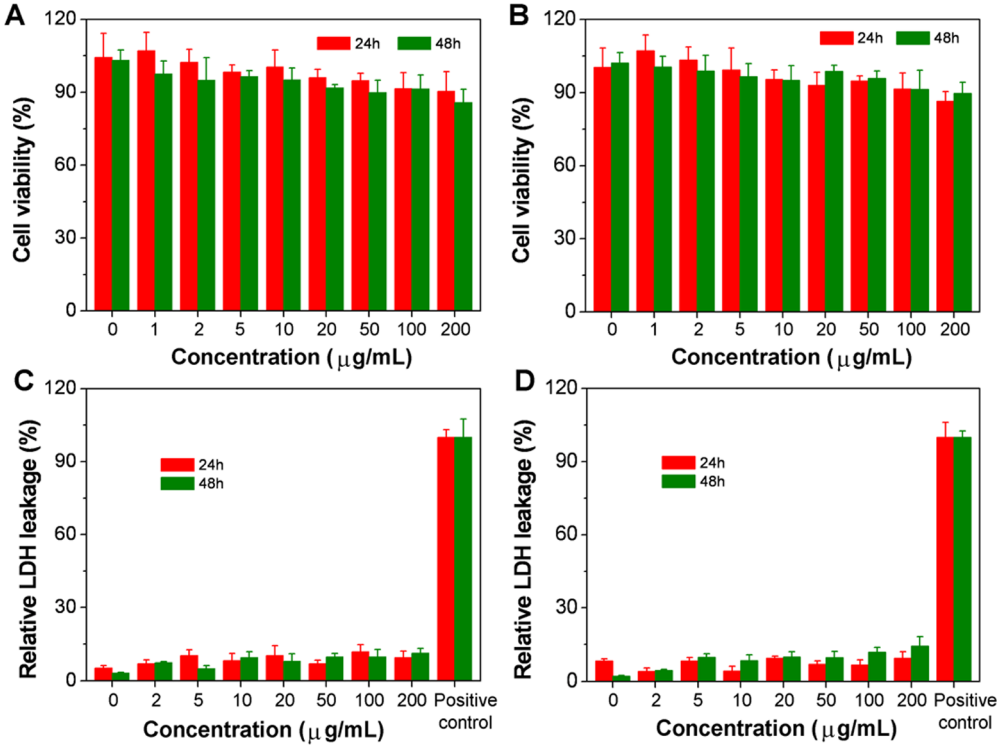

Figure 6. Relative viabilities of U87-MG (A) and MCF-7 (B) cells incubated with TCP NPs for 24 and 48 h. Relative LDH leakage from U87-MG (C) and MCF-7 (D) cells incubated with TCP NPs for 24 and 48 h. Positive controls indicate cells treated with 1% Triton X-100.

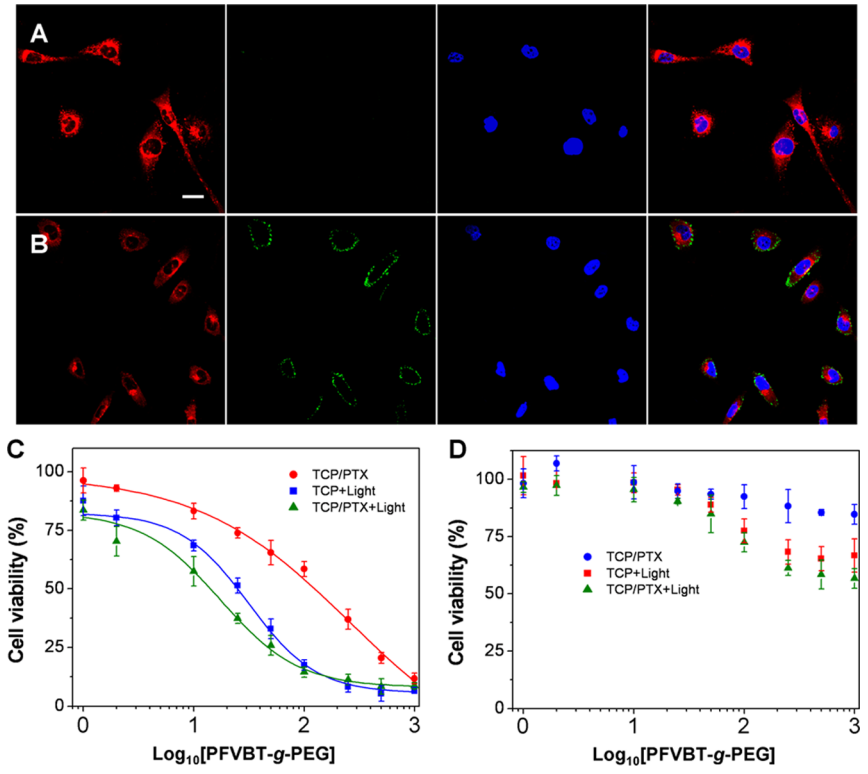

Figure 7. Cell apoptosis imaging using FITC-tagged Annexin V without (A) and with (B) light irradiation. The images can be classified to red fluorescence from CPE, green fluorescence from FITC-tagged Annexin V, blue fluorescence from the nuclei of cells dyed by Hoechst 33342, and the overlay images of above. The scale bar is 20 μm. Inhibition of U87-MG (C) and MCF-7 (D) cells growth with different concentrations of TCP/PTX NPs without light irradiation, TCP NPs with light irradiation (10 min), and TCP/PTX NPs with light irradiation (10 min) after incubation with the cells for 24 h. The loading capacity of PTX in TCP/PTX NPs is 4.9%.

dx.doi.org/10.1021/am5020925 | ACS Appl. Mater. Interfaces 2014, 6, 14903−14910

integrity study demonstrate that the TCP NPs have no obvious toxicity to cells, which is desirable for biomedical applications.

Apoptosis is the process of programmed cell death. FITC-tagged Annexin V has been widely used as the fluorescent probe to distinguish viable cells from apoptotic ones. It can bind to the membrane of apoptotic cells that express phosphatidylserine. As shown in Figure 7A, before the light irradiation, there is no FITC signal detectable in U87-MG cells, indicating no cell apoptosis. However, after the light irradiation, FITC signals are clearly observed from the cell membrane, indicating that the cells undergo apoptosis process. Further quantitative evaluation of the therapeutic effect of TCP/PTX NPs (The loading capacity of PTX in TCP/PTX NPs is 4.9%) with different treatments was studied by standard MTT assay. As shown in Figure 7C, when incubated with U87-MG cells, TCP/PTX NPs with light irradiation (10 min, 0.1 W cm^{-2}) mediated the highest rate of cell viability inhibition compared to the single treatment of TCP/PTX NPs without light irradiation (chemotherapy) or TCP NPs with light irradiation (photodynamic therapy). The IC_{50} of U87-MG cells incubated with TCP/PTX NPs with light irradiation for combination therapy is 12.7 $\mu g\ mL^{-1}$, while the IC_{50} for the solely chemotherapy and photodynamic therapy is 132.8 $\mu g\ mL^{-1}$ (for PTX, the concentration is 6.6 $\mu g\ mL^{-1}$) and 25.5 $\mu g\ mL^{-1}$, respectively. The combination index (CI) was calculated according to the previous report.[32] In this work, the CI value is calculated to be 0.61 (<1), which demonstrates the synergistic effect of TCP/PTX NPs for chemotherapy and photodynamic therapy. For MCF-7 cells, due to the inefficient cellular uptake of TCP/PTX NPs, no significant cytotoxicity was observed (Figure 7D).

CONCLUSIONS

In summary, we fabricated PTX-loaded nanoparticles based on a PEGylated CPE for imaging guided combination of chemo- and photodynamic cancer therapy. In this system, the CPE not only served as a matrix for drug carrier but also as photosensitizer for PDT. To improve the tumor specificity of the system, targeted moiety was modified to the surface of the self-assembled CP/PTX NPs. Cell viability studies revealed that the combination of chemo- and PDT resulted in higher toxicity than each treatment alone. The drug delivery system based on PEGylated CPE is simple to design and synthesize, which offers new opportunities for image-guided photodynamic and chemotherapy with enhanced therapeutic effects in cancer treatment. Currently, we are working on the design of new CPE based photosensitizers with longer absorption wavelength for potential in vivo application.

AUTHOR INFORMATION

Corresponding Author

*Email: cheliub@nus.edu.sg.

Notes

The authors declare no competing financial interest.

ACKNOWLEDGMENTS

We thank the Singapore National Research Foundation (R-279-000-390-281), the SMART (R279-000-378-592), Ministry of Defense (R279-000-340-232), and the Institute of Materials Research and Engineering of Singapore (IMRE/12-8P1103) for financial support.

REFERENCES

(1) Langer, R. Drug Delivery and Targeting. *Nature* **1998**, *392*, 5−10.
(2) Brannon-Peppas, L.; Blanchette, J. O. Nanoparticle and Targeted Systems for Cancer Therapy. *Adv. Drug Delivery Rev.* **2004**, *56*, 1649−1659.
(3) Petros, R. A.; DeSimone, J. M. Strategies in the Design of Nanoparticles for Therapeutic Applications. *Nat. Rev. Drug Discovery* **2010**, *9*, 615−627.
(4) Couleaud, P.; Morosini, V.; Frochot, C.; Richeter, S.; Raehm, L.; Durand, J. O. Silica-Based Nanoparticles for Photodynamic Therapy Applications. *Nanoscale* **2010**, *2*, 1083−1095.
(5) Wang, C.; Cheng, L.; Liu, Z. Upconversion Nanoparticles for Photodynamic Therapy and Other Cancer Therapeutics. *Theranostics* **2013**, *3*, 317−330.
(6) Shibu, E. S.; Hamada, M.; Murase, N.; Biju, V. Nanomaterials Formulations for Photothermal and Photodynamic Therapy of Cancer. *J. Photochem. Photobiol., C* **2013**, *15*, 53−72.
(7) Szakacs, G.; Paterson, J. K.; Ludwig, J. A.; Booth-Genthe, C.; Gottesman, M. M. Targeting Multidrug Resistance in Cancer. *Nat. Rev. Drug Discovery* **2006**, *5*, 219−234.
(8) Hu, C. M.; Aryal, S.; Zhang, L. Nanoparticle-Assisted Combination Therapies for Effective Cancer Treatment. *Ther. Delivery* **2010**, *1*, 323−334.
(9) Sun, T. M.; Du, J. Z.; Yao, Y. D.; Mao, C. Q.; Dou, S.; Huang, S. Y.; Zhang, P. Z.; Leong, K. W.; Song, E. W.; Wang, J. Simultaneous Delivery of siRNA and Paclitaxel via a "Two-In-One" Micelleplex Promotes Synergistic Tumor Suppression. *ACS Nano* **2011**, *5*, 1483−1494.
(10) Gong, H.; Cheng, L.; Xiang, J.; Xu, H.; Feng, L.; Shi, X.; Liu, Z. Near-Infrared Absorbing Polymeric Nanoparticles as a Versatile Drug Carrier for Cancer Combination Therapy. *Adv. Funct. Mater.* **2013**, *23*, 6059−6067.
(11) Lee, S. M.; O'Halloran, T. V.; Nguyen, S. T. Polymer-Caged Nanobins for Synergistic Cisplatin-Doxorubicin Combination Chemotherapy. *J. Am. Chem. Soc.* **2010**, *132*, 17130−17138.
(12) Dolmans, D.; Fukumura, D.; Jain, R. K. Photodynamic Therapy for Cancer. *Nat. Rev. Cancer.* **2003**, *3*, 380−387.
(13) Castano, A. P.; Mroz, P.; Wu, M. X.; Hamblin, M. R. Photodynamic Therapy Plus Low-Dose Cyclophosphamide Generates Antitumor Immunity in a Mouse Model. *Proc. Natl. Acad. Sci. U.S.A.* **2008**, *105*, 5495−5500.
(14) Khdair, A.; Di, C.; Patil, Y.; Ma, L.; Dou, Q. P.; Shekhar, M. E.; Panyam, J. Nanoparticle-Mediated Combination Chemotherapy and Photodynamic Therapy Overcomes Tumor Drug Resistance. *J. Controlled Release* **2010**, *141*, 137−144.
(15) Peterson, C. M.; Lu, J. M.; Sun, Y.; Peterson, C. A.; Shiah, J. G.; Straight, R. C.; Kopecek, J. Combination Chemotherapy and Photodynamic Therapy with *N*-(2-hydroxypropyl) Methacrylamide Copolymer-Bound Anticancer Drugs Inhibit Human Ovarian Carcinoma Heterotransplanted in Nude Mice. *Cancer. Res.* **1996**, *56*, 3980−3985.
(16) Peng, C. L.; Lai, P. S.; Lin, F. H.; Yueh-Hsiu, W. S.; Shieh, M. J. Dual Chemotherapy and Photodynamic Therapy in an HT-29 Human Colon Cancer Xenograft Model using SN-38-loaded Chlorin-Core Star Block Copolymer Micelles. *Biomaterials* **2009**, *30*, 3614−3625.
(17) Son, K. J.; Yoon, H. J.; Kim, J. H.; Jang, W. D.; Lee, Y.; Koh, W. G. Photosensitizing Hollow Nanocapsules for Combination Cancer Therapy. *Angew. Chem., Int. Ed.* **2011**, *50*, 11968−11971.
(18) Wang, C.; Cheng, L.; Liu, Y.; Wang, X.; Ma, X.; Deng, Z.; Li, Y.; Liu, Z. Imaging-Guided pH-Sensitive Photodynamic Therapy Using Charge Reversible Upconversion Nanoparticles under Near-Infrared Light. *Adv. Funct. Mater.* **2013**, *23*, 3077−3086.
(19) Zhu, C.; Liu, L.; Yang, Q.; Lv, F.; Wang, S. Water-Soluble Conjugated Polymers for Imaging, Diagnosis, and Therapy. *Chem. Rev.* **2012**, *112*, 4687−4735.
(20) Jiang, H.; Taranekar, P.; Reynolds, J. R.; Schanze, K. S. Conjugated Polyelectrolytes: Synthesis, Photophysics, and Applications. *Angew. Chem., Int. Ed.* **2009**, *48*, 4300−4316.

(21) Liu, B.; Bazan, G. C. Homogeneous Fluorescence-Based DNA Detection with Water-Soluble Conjugated Polymers. *Chem. Mater.* **2004**, *16*, 4467−4476.
(22) Pu, K. Y.; Liu, B. Fluorescent Conjugated Polyelectrolytes for Bioimaging. *Adv. Funct. Mater.* **2011**, *21*, 3408−3423.
(23) Feng, G.; Ding, D.; Liu, B. Fluorescence Bioimaging with Conjugated Polyelectrolytes. *Nanoscale* **2012**, *4*, 6150−6165.
(24) Yuan, Y.; Ding, D.; Li, K.; Liu, J.; Liu, B. Tumor-Responsive Fluorescent Light-up Probe Based on a Gold Nanoparticle/Conjugated Polyelectrolyte Hybrid. *Small* **2014**, *10*, 1967−1975.
(25) Duan, X.; Liu, L.; Feng, X.; Wang, S. Assemblies of Conjugated Polyelectrolytes with Proteins for Controlled Protein Photoinactivation. *Adv. Mater.* **2010**, *22*, 1602−1606.
(26) Yuan, H.; Chong, H.; Wang, B.; Zhu, C.; Liu, L.; Yang, Q.; Lv, F.; Wang, S. Chemical Molecule-Induced Light-Activated System for Anticancer and Antifungal Activities. *J. Am. Chem. Soc.* **2012**, *134*, 13184−13187.
(27) Corbitt, T. S.; Sommer, J. R.; Chemburu, S.; Ogawa, K.; Ista, L. K.; Lopez, G. P.; Whitten, D. G.; Schanze, K. S. Conjugated Polyelectrolyte Capsules: Light-Activated Antimicrobial Micro-"Roach Motels". *ACS Appl. Mater. Interfaces* **2009**, *1*, 48−52.
(28) Hersel, U.; Dahmen, C.; Kessler, H. RGD Modified Polymers: Biomaterials for Stimulated Cell Adhesion and Beyond. *Biomaterials* **2003**, *24*, 4385−4415.
(29) Pu, K. Y.; Cai, L.; Liu, B. Design and Synthesis of Charge-Transfer-Based Conjugated Polyelectrolytes as Multicolor Light-Up Probes. *Macromolecules* **2009**, *42*, 5933−5940.
(30) Pu, K. Y.; Li, K.; Liu, B. A Molecular Brush Approach to Enhance Quantum Yield and Suppress Nonspecific Interactions of Conjugated Polyelectrolyte for Targeted Far-Red/Near-Infrared Fluorescence Cell Imaging. *Adv. Funct. Mater.* **2010**, *20*, 2770−2777.
(31) Bourre, L.; Thibaut, S.; Briffaud, A.; Rousset, N.; Eleouet, S.; Lajat, Y.; Patrice, T. Indirect Detection of Photosensitizer Ex Vivo. *J. Photochem. Photobiol., B* **2002**, *67*, 23−31.
(32) Wang, Y.; Wang, K.; Zhao, J.; Liu, X.; Bu, J.; Yan, X.; Huang, R. Multifunctional Mesoporous Silica-Coated Graphene Nanosheet Used for Chemo-Photothermal Synergistic Targeted Therapy of Glioma. *J. Am. Chem. Soc.* **2013**, *135*, 4799−4804.